ETH zürich

ETH Library

Decoupling porosity and compositional effects on desilicated ZSM-5 zeolites for optimal alkylation performance

Journal Article

Author(s):
Milina, Maria; Mitchell, Sharon; Trinidad, Zair D.; Verboekend, Danny; Pérez-Ramírez, Javier

Publication date:
2012-04-01

Permanent link:
https://doi.org/10.3929/ethz-a-010782786

Rights / license:
In Copyright - Non-Commercial Use Permitted

Originally published in:
Catalysis Science & Technology 2(4), https://doi.org/10.1039/c2cy00456a

Funding acknowledgement:
134572 - A fundamental approach to the scale up of hierarchical zeolite catalysts (SNF)

This page was generated automatically upon download from the ETH Zurich Research Collection.
For more information, please consult the Terms of use.

Journal Name

Dynamic Article Links ►

Cite this: DOI: 10.1039/c0xx00000x

www.rsc.org/xxxxxx

PAPER

Decoupling porosity and compositional effects in desilicated ZSM-5 for optimal alkylation performance

Maria Milina, Sharon Mitchell, Zair Domínguez Trinidad, Danny Verboekend and Javier Pérez-Ramírez*

Received (in XXX, XXX) Xth XXXXXXXXX 20XX, Accepted Xth XXXXXXXXX 20XX
DOI: 10.1039/b000000x

Desilication of conventional zeolites in alkaline medium generates intracrystalline mesoporosity, but inevitably changes other properties such as the Si/Al ratio and aluminium distribution. Assessing the individual effects of porosity, composition, and acidity on the catalytic performance of desilicated zeolites is relevant for their optimal design. Herein, we decouple the respective impacts in the acid-catalysed alkylation of toluene (or cyclohexylbenzene) with benzyl alcohol. These reactions experience strong accessibility constraints to the micropores, providing high sensitivity to the properties of the developed mesopore surface. Through strategic comparison of alkaline-treated ZSM-5 zeolites prepared with and without subsequent acid treatment, we show that while acidity is important, the alkylation activity is dominated by the mesoporous surface area. The selectivity to (methylbenzyl)benzene does not depend on the available external surface. Large mesopore volumes offer no catalytic benefit, and variation in micropore volume has a minimal effect. Acid-treated mesoporous zeolites exhibit higher catalytic activities primarily due to textural enhancements by removal of aluminium-rich amorphous debris. The catalytic results are rationalised on the basis of extensive characterisation (AAS, N_2 sorption, XRD, TEM, ^{27}Al MAS NMR, FTIR, NH_3-TPD) and adsorption of toluene and cyclohexylbenzene.

1. Introduction

Zeolites are a unique class of crystalline microporous materials owing to their high surface area, strong acidity, shape selectivity, and thermal stability. However, active sites confined within their micropores are often inefficiently used due to diffusion constraints.[1] Performance enhancements observed on application of hierarchical (mesoporous) zeolites, possessing a complementary network of mesopores, have attracted widespread attention.[2-6]

Interconnected mesopores can be efficiently introduced in a scalable manner by desilication of zeolites in alkaline media.[7,8] A major concern of post-synthetic methods are the compositional changes experienced during demetallation.[7] Upon alkaline treatment, silicon is preferentially extracted into solution, while aluminium species realuminate on the external surface, playing an important role in pore direction.[9,10] Alkaline-treated zeolites exhibit a decreased bulk Si/Al ratio, micropore volume and crystallinity, and an increased amount of Lewis acid sites.[11-16]

To avoid possible alteration of the catalytic properties arising from alkali-induced surface realumination, sequential acid treatments are increasingly applied. The additional step aims to restore the original framework composition.[9,10] Acid washing of alkaline-leached ZSM-5 is accompanied by simultaneous enhancements in micropore volume, mesoporous surface area, and crystallinity.[11] These concomitant changes were never systematically studied in catalysed reactions. As such the implications of realuminated species are still not fully understood. This is particularly true for zeolites of low Si/Al ratio at high base concentrations, where larger amounts of aluminium-rich amorphous debris are generated.[11]

Herein, the alkylations of toluene and cyclohexylbenzene with benzyl alcohol (Scheme 1) are taken as model reactions to decouple the relative impacts of compositional and porosity effects in desilicated zeolites. Mesoporous ZSM-5 zeolites have been advantageously applied for both the alkylation[17-19] and the related acylation[20] of aromatic molecules. The choice of access-limited reactions provides optimal sensitivity to the redistribution of aluminium on alkaline treatment and acid washing through confinement of the alkylation activity to the mesoporous surface. Property-function relationships are established through detailed sample characterisation using multiple techniques. We address important design aspects of mesoporous zeolites such as the aluminium content and acid site speciation, the optimal extent and appropriate descriptors of mesoporosity, and the impact of residual aluminium-rich species on adsorption and catalysis.

2. Experimental

2.1. Post-synthetic treatments

Various commercial ZSM-5 zeolites were obtained in the ammonium form: Z10 (PZ2/23, Zeochem), Z15 (CBV 3024E, Zeolyst International), Z25 (CBV 5524G, Zeolyst International),

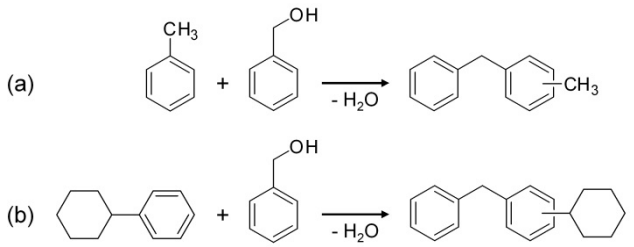

Scheme 1 Alkylation of (a) toluene and (b) cyclohexylbenzene with benzyl alcohol.

Z40 (CBV 8014, Zeolyst International), and Z200 (PZ2/400, Zeochem). The *x* in the code Z*x* refers to the nominal Si/Al ratio according to manufacturers' specifications. The zeolites were converted into the protonic form by calcination in static air at 823 K for 5 h using a heating rate of 5 K min^{-1}. The parent samples (coded P) were treated in aqueous NaOH solution (0.1-0.7 M, 30 cm^3 per gram of zeolite) using an Easymax™ 102 reactor system (Mettler Toledo). Following zeolite addition, the alkaline solution, heated at 338 K, was stirred for 30 min. The treatment was quenched using an ice-water mixture, and the solids were collected by vacuum filtration, washed extensively with distilled water, and dried at 338 K. Selected alkaline-treated samples were treated in aqueous HCl solution (0.02-0.1 M, 100 cm^3 per gram of zeolite) at 338 K for 6 h. The alkaline- and acid-treated zeolites were converted into the protonic form by three consecutive ion exchanges in aqueous NH_4NO_3 solution (0.1 M, 298 K, 12 h, 100 cm^3 per gram of zeolite), followed by the above-described calcination step. Steaming was carried out in a quartz fixed-bed reactor (9 mm i.d.) with a shallow bed of zeolite powder at ambient pressure. The zeolite was treated in a flow of water vapour and N_2 at 873 K for 5 h (30 cm^3 min^{-1} N_2, H_2O partial pressure of 300 mbar). Along the manuscript, the codes AT, AW, and ST denote alkaline treatment, acid washing, and steaming, respectively.

2.2. Characterisation methods

Chemical composition of the samples was determined by atomic absorption spectroscopy (AAS) using a Varian SpectrAA 220 FS spectrometer. N_2 sorption isotherms at 77 K were measured in a Quantachrome Quadrasorb-SI gas adsorption analyser. Prior to the measurement, the samples were degassed in vacuum at 573 K for 10 h. X-ray diffraction (XRD) was undertaken using a PANalytical X'Pert PRO-MPD diffractometer operated in Bragg-Brentano geometry using Ni-filtered Cu Kα radiation (λ = 0.1541 nm). Data were recorded in the range 5-50° 2θ with an angular step size of 0.05° and a counting time of 8 s per step. ^{27}Al magic angle spinning nuclear magnetic resonance (MAS NMR) spectra were recorded at a spinning speed of 12 kHz on a Bruker AVANCE 400 NMR spectrometer equipped with a 4 mm probe head and 4 mm ZrO_2 rotors at 104.3 MHz. ^{27}Al spectra were measured using 4096 accumulations, 1 µs pulses, a recycle delay of 0.5 s, and $(NH_4)Al(SO_4)_2{\cdot}12H_2O$ as the reference. Transmission electron microscopy (TEM) was performed with a Phillips CM12 microscope operated at 100 kV. Infrared spectroscopy was performed at 473 K under a N_2 atmosphere using a Thermo Nicolet 5700 spectrometer equipped with a SpectraTech Collector II diffuse reflectance accessory and a high-temperature cell. Prior to the measurement, the sample was dried at 573 K under a N_2 flow (100 cm^3 min^{-1}) for 60 min. Spectra were recorded in the range of 650-4000 cm^{-1} with a nominal resolution of 4 cm^{-1} and a co-addition of 200 scans. Temperature-programmed desorption of ammonia (NH_3-TPD) was carried out in a Thermo TPDRO 1100 unit equipped with a thermal conductivity detector. The zeolite powder (0.1 g) was pretreated at 823 K in He flow (20 cm^3 min^{-1}) for 2 h. Afterwards, 10 vol.% NH_3 in He (20 cm^3 min^{-1}) was adsorbed at 473 K for 30 min followed by He purging at the same temperature for 1 h. This procedure was repeated three times. Desorption of NH_3 was monitored in the range 473-973 K using a heating rate of 10 K min^{-1}. The adsorption isotherms of toluene and cyclohexylbenzene were measured in an Intelligent Gravimetric Analyser (IGA-002, Hiden Analytical) at 298 and 320 K, respectively. Prior to analysis, the samples (10 mg) were outgassed at 573 K for 10 h. The upper pressure limit was determined by the saturated vapour pressure of toluene and cyclohexylbenzene (38 mbar and 0.37 mbar, respectively), which was estimated using the Antoine equation with the component-specific constants reported elsewhere.[21,22]

2.3. Catalytic tests

The alkylation of toluene or cyclohexylbenzene with benzyl alcohol was conducted in an Endeavor® Catalyst Screening System (Argonaut Technologies), consisting of 8 parallel reactors with a working volume of 5 cm^3. The powdered catalyst (25 mg, pre-dried at 573 K for 2 h) was added to a mixture containing toluene (47 mmol, Fluka, 99.7%) or cyclohexylbenzene (0.4 mmol, ABCR, 98%), benzyl alcohol (0.6 mmol, Aldrich, 99.9%), and ethylycyclohexane (0.2 mmol, Acros, > 99%) which acted as an internal standard. The reactor was then sealed, pressurised to 5 bar, and heated to 433 K. On reaching the desired temperature, the reaction mixture was mechanically stirred (1000 rpm) by overhead impellers. Following the desired reaction time, the reactors were cooled and liquid samples were analysed using a gas chromatograph (HP 6890) equipped with a HP5 capillary column and a flame ionization detector (FID).

3. Results and discussion

3.1. Alkylation over conventional zeolites

Table 1 summarises the chemical composition and textural properties of the commercial H-ZSM-5 zeolites. Sharp reflections corresponding to the MFI structure were measured by XRD (not shown). As illustrated for Z15-P and Z40-P in Fig. 1, the type I N_2 sorption isotherms confirmed their microporous character. The corresponding micropore volumes (V_{micro}) and low-to-moderate external surface areas (S_{meso}) estimated are typical of ZSM-5. No evidence of intracrystalline mesoporosity was visible by TEM (not shown), or by analysis of the BJH pore size distributions (inset, Fig. 1). ^{27}Al MAS NMR spectra showed that the zeolites contained predominantly tetrahedral aluminium (band at 59 ppm in Fig. 2). Only a small but identifiable proportion of octahedral aluminium, in extra-framework positions (band centred at0 ppm), was observed for zeolites with low Si/Al ratios. The increased intensities of the high-temperature desorption peak (> 700 K), in the NH_3-TPD profile (Fig. 3), and of the absorbance

This journal is © The Royal Society of Chemistry [year]

Table 1 Treatment conditions and physico-chemical characterisation of parent and modified ZSM-5 zeolites.

Sample	NaOH (M)	HCl (M)	Yield (%)	Si/Al[a] (-)	S_{meso}[b] (m^2 g^{-1})	S_{BET}[c] (m^2 g^{-1})	V_{micro}[b] (cm^3 g^{-1})	V_{meso}[d] (cm^3 g^{-1})
Z10-P	-	-	-	-	102	394	0.12	0.34
Z15-P	-	-	-	15	76	412	0.14	0.15
Z15-ST	-	-	100	15	112	415	0.13	0.23
Z15-AT1	0.6	-	70	10	147	444	0.13	0.38
Z15-AT1-AW1	0.6	0.02	94 (66)[e]	12	158	588	0.15	0.40
Z25-P	-	-	-	25	76	461	0.17	0.31
Z40-P	-	-	-	39	78	468	0.17	0.28
Z40-ST	-	-	100	39	72	456	0.17	0.13
Z40-AT1	0.1	-	84	34	135	497	0.15	0.19
Z40-AT1-AW2	0.1	0.1	95 (80)	34	135	498	0.15	0.21
Z40-AT2	0.2	-	67	25	288	589	0.13	0.40
Z40-AT2-AW2	0.2	0.1	91 (61)	32	296	573	0.12	0.46
Z40-AT3	0.3	-	45	17	417	637	0.09	0.78
Z40-AT3-AW2	0.3	0.1	89 (40)	32	440	675	0.10	0.84
Z40-AT3-AW2-ST	0.3	0.1	100 (40)	32	484	648	0.06	0.96
Z40-AT4	0.5	-	18	7	336	519	0.08	0.98
Z40-AT4-AW2	0.5	0.1	85 (15)	-	415	635	0.09	1.00
Z40-AT5	0.7	-	11	4	294	349	0.02	0.94
Z40-AT5-AW2	0.7	0.1	69 (8)	-	381	639	0.11	1.02
Z200-P	-	-	-	-	73	398	0.15	0.24

[a] AAS. [b] *t*-plot method. [c] BET method. [d] $V_{meso} = V_{pore} - V_{micro}$. [e] values in parentheses represent the overall yield (alkaline treatment and acid washing). The code of the samples includes the nominal Si/Al molar ratio of starting zeolites and the treatment conducted: AT (alkaline treatment), AW (acid washing), and ST (steaming). P refers to the parent sample.

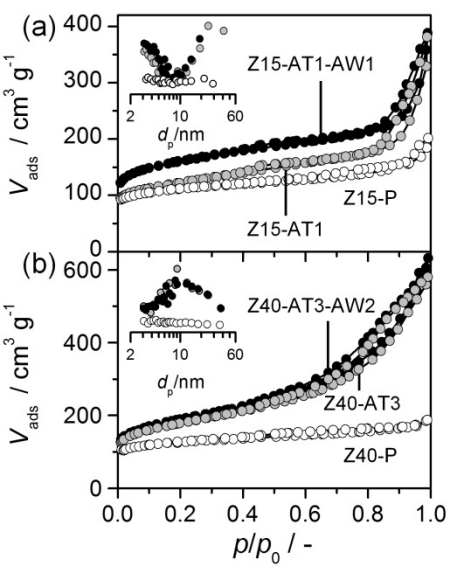

Fig. 1 N_2 isotherms of selected zeolites. Insets: BJH mesopore size distributions.

at 3600 cm^{-1}, in the hydroxyl stretching region of the IR spectra (Fig. 4), are consistent with an increased concentration of strong (Brønsted) acid sites at lower Si/Al ratios. The catalytic dependence on framework composition and related acidity was verified by assessing the performance of the parent zeolites in the alkylation of toluene with benzyl alcohol. The conversion of benzyl alcohol (X_{BA}) increased linearly with the aluminium content (Fig. 5). High-silica Z200-P was catalytically inactive

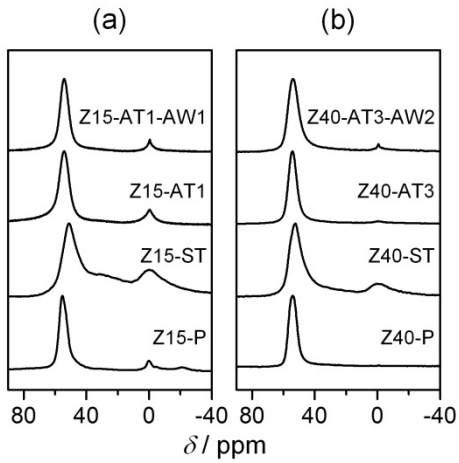

Fig. 2 ^{27}Al MAS NMR spectra of selected zeolites.

under the conditions studied.

The steam-induced extraction of framework aluminium permits determination of the influence of acidity modification on the alkylation activity. Following steam treatment, no major variation in sample porosity was observed (Table 1). The ^{27}Al MAS NMR spectra, however, evidenced an increased intensity of the band at 0 ppm, and the appearance of an additional broad signal visible as a shoulder to the band at 59 ppm in the steamed zeolites (Fig. 2). These observations are related to dealumination of the framework, the condensation of dislodged aluminium as extra-framework species, and to greater variation in the coordination environment of the remaining lattice

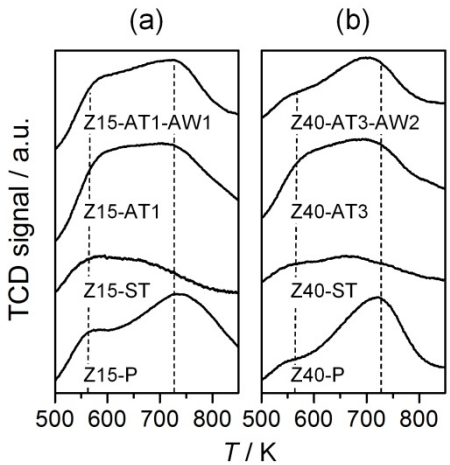

Fig. 3 NH_3-TPD profiles of selected zeolites.

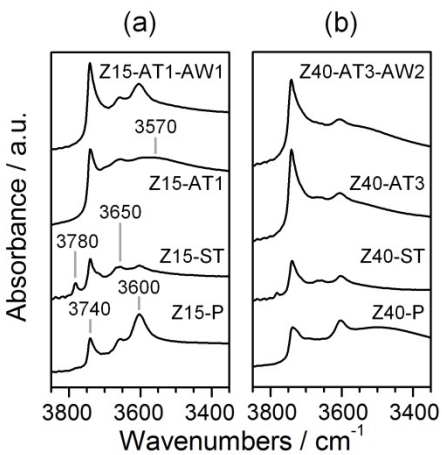

Fig. 4 FTIR spectra of selected zeolites.

aluminium.[23,24] Accordingly, a decrease in the infrared absorbance at 3600 cm^{-1} (associated with Brønsted acid sites)[25] and an increase in the absorbances at 3650 cm^{-1} and at 3780 cm^{-1} (associated with extra-framework aluminium species)[25] were seen in the FTIR spectrum of Z15-ST and Z40-ST (Fig. 4). Furthermore, the contribution above 700 K in the NH_3-TPD profiles vanished (Fig. 3). No benzyl alcohol conversion was observed over the steamed zeolites (Fig. 5), strongly suggesting that weakly acidic extra-framework aluminium is not catalytically active.

3.2. Post-synthetic modification by alkaline and acid treatments

In view of the acidity requirement identified in Section 3.1, the Z15-P and Z40-P samples were selected for the preparation of hierarchical zeolites by post-synthetic modification. We have previously mapped out the range of achievable porous properties in MFI zeolites on variation of the base concentration during alkaline treatment and when treating parent zeolites with differing Si/Al ratios.[11] For aluminium-rich zeolites (*e.g.* Si/Al = 15), the great importance of subsequent acid washing to increase the micropore volume and mesoporous surface area and to restore the bulk Si/Al ratio of the parent zeolites, was also shown. Taking

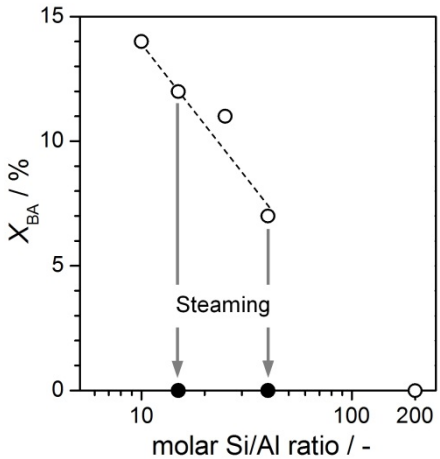

Fig. 5 Influence of the molar Si/Al ratio of the parent zeolites on the conversion of benzyl alcohol (BA) after 25 min in the alkylation with toluene (T). The zero conversion on the steamed zeolites is indicated by the solid symbols. Conditions: T = 433 K, P = 5 bar, T/BA = 80, 0.6 wt.% zeolite.

these observations into account, a number of hierarchical zeolites with distinct properties were prepared, characterised, and evaluated in the liquid-phase alkylation of aromatics. The corresponding chemical composition, porous properties, and treatment yields, are collected in Table 1.

Alkaline treatment

Upon alkaline treatment of Z15-P and Z40-P mesoporous surface areas were developed in the range of 76-147 $m^2\,g^{-1}$ and 78-417 $m^2\,g^{-1}$, respectively (Table 1). As reported previously,[11] treatment of the zeolite with lower aluminium content (Z40-P) and at higher NaOH concentration led to decreased yields. Detailed characterisation is illustrated for Z15-AT1 and Z40-AT3, the hierarchical zeolites which exhibited the highest S_{meso}.

The introduction of mesoporosity was clearly reflected in the N_2 adsorption isotherms, by an enhanced uptake at intermediate and high relative pressures (Fig. 1). Analysis of the BJH pore size distributions (Fig. 1, inset) evidenced mesopore sizes centred around 10 nm for Z40-AT3. For Z15-AT1, a broader mesopore size distribution was observed. The intracrystalline origin of the mesoporosity has been confirmed by TEM (not shown). Due to the higher external area, the intensity of the silanol band at 3740 cm^{-1} in the IR spectra of desilicated samples increased (Fig. 4). The XRD patterns of the treated zeolites evidenced retention of the MFI structure in all cases (not shown).

Modification of the porous properties was accompanied by a reduction in the bulk Si/Al ratios (Table 1). No indication of an increase in the number of Brønsted acid sites is evidenced by IR spectroscopy (Fig. 4). The rise in the intensity of the low-temperature contribution (*ca.* 570 K) in the NH_3-TPD profile(Fig. 3), reveals an increased presence of sites of moderate acidic strength, which are thought to be Lewis-type and concentrated at the mesopore surface.[26,27] No substantial evidence of octahedrally-coordinated aluminium was observed in the ^{27}Al MAS NMR (Fig. 2) or IR (Fig. 4) spectra, indicating the

This journal is © The Royal Society of Chemistry [year]

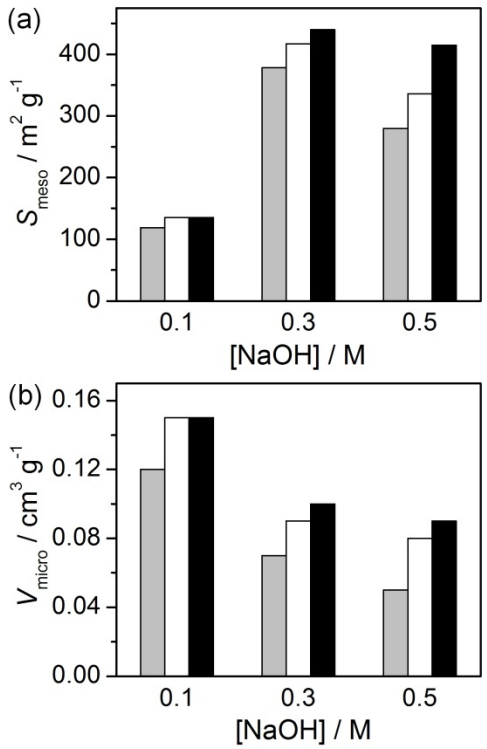

Fig. 6 Influence of ion exchange and acid washing on the porous properties of desilicated Z40 zeolites, treated at different NaOH concentrations. Alkaline-treated zeolites are represented by grey bars, sequentially alkaline-treated and ion-exchanged zeolites by open bars, and sequentially alkaline-treated and acid-washed zeolites by open and solid bars.

different nature in comparison with the extra-framework aluminium formed upon steaming.

Acid treatment

The subsequent application of a mild acid treatment increased the molar Si/Al ratios to values similar to those of their parent counterparts (Table 1). As treatment of the conventional zeolites under equivalent conditions did not extract framework aluminium,[11,28] this was primarily attributed to the removal of deposited aluminium-rich debris. Consistently, the crystallinity, micropore volume, and mesoporous surface area of acid washed zeolites (Z15-AT1-AW1 and Z40-AT3-AW2) increased (Table 1). Furthermore, a reduction in the low temperature desorption peak in the NH_3-TPD profile (Fig. 3) and the improved visibility of the Brønsted hydroxyl stretch in the IR spectrum (Fig 4a), confirmed a decrease in the number of moderately acidic sites. No significant changes were evident in the ^{27}Al MAS NMR spectra compared with the alkaline-treated sample (Fig. 2).

The mild acidic conditions (pH ~ 5) of ion-exchange (with aqueous ammonium nitrate) also contribute to variation in the porous properties. The relative enhancement in V_{micro} and S_{meso} brought about by ion exchange and acid washing of alkaline-treated zeolites are compared in Fig. 6. For the zeolite desilicated at low base concentration (0.1 M NaOH), similar improvements

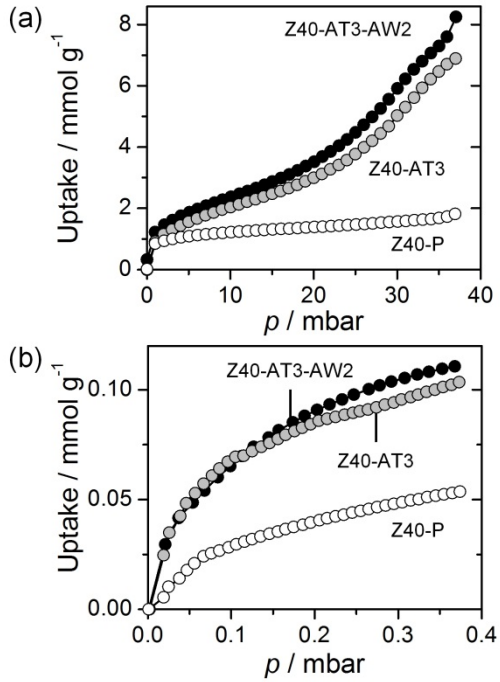

Fig. 7 Adsorption isotherms of (a) toluene at 298 K and (b) cyclohexylbenzene at 321 K on parent and mesoporous zeolites.

were seen for both treatments. The micropore volume was most significantly affected, increasing from 0.12 to 0.15 cm^3 g^{-1}, owing to the exchange of charge-balancing and to the removal of residual sodium ions. Only minor variation in the mesoporous surface area was observed. In contrast for the zeolite desilicated at higher base concentration (0.5 M NaOH) acid washing was more beneficial improving S_{meso} by 135 m^2 g^{-1} with respect to the 56 m^2 g^{-1} increase induced by ion exchange.

3.3. Adsorption and diffusion properties

Further to the above described physico-chemical characterisation, the adsorption properties of Z40-P, Z40-AT3, and Z40-AT3-AW2 were assessed with respect to toluene and cyclohexylbenzene, the reagents subsequently used in the catalytic study.

The toluene adsorption isotherm of the parent Z40-P exhibited a single sharp uptake at low pressure ($p < 2$ mbar), related to micropore filling and characteristic of type I behaviour (Fig. 7a). The mesoporous zeolites displayed slightly higher initial uptakes of toluene compared to the parent sample. In contrast, analysis by N_2 adsorption evidenced lower micropore volumes (0.10 cm^3 g^{-1} compared to 0.17 cm^3 g^{-1}, respectively). This demonstrates an additional adsorption contribution, which should be related to the mesopore introduction. At higher pressures the adsorbed amount increased progressively. The uptake of the Z40-AT3-AW2 was higher than that of Z40-AT3 at all relative pressures, consistent with the enhanced textural properties of the washed sample. Assuming a bulk liquid density of toluene, the total pore volumes estimated are similar to those derived from N_2 adsorption. This indicates that both the micro- and mesopores were completely filled, confirming their full accessibility.

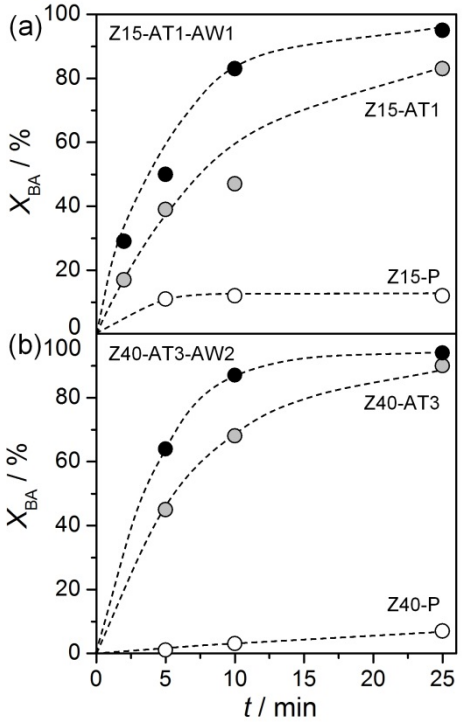

Fig. 8 Influence of post-synthetic modification on the conversion of benzyl alcohol in the alkylation with toluene. Reaction conditions as in caption of Fig. 5.

For the larger cyclohexylbenzene, which is not expected to penetrate into the micropores, significantly lower uptakes were observed for all zeolites (Fig. 7b). The mesoporous samples exhibited higher uptakes that the parent zeolite. In contrast to the adsorption of toluene, the initial adsorption of cyclohexylbenzene was similar for both the alkaline-treated and acid-washed zeolites, reflecting the negligible impact of micropore volume. However, the higher mesoporosity of the washed sample resulted in increased uptake at higher pressures.

3.4. Alkylation over hierarchical ZSM-5

Fig. 8 displays the activity enhancements achieved in the alkylation of toluene with benzyl alcohol over the alkaline-treated zeolites, possessing the highest mesoporous surface areas (Z15-AT1 and Z40-AT3), with respect to their purely microporous counterparts (Z15-P and Z40-P). Following 25 min of reaction, the corresponding benzyl alcohol conversions were 12 and 83%, for Z15-P and Z15-AT1, and 7 and 90%, for Z40-P and Z40-AT3, respectively. The gain in catalytic activity on application of the acid-washed hierarchical zeolites, is also shown. This effect was greater for Z15-AT1 than Z40-AT3 in line with the increased presence of aluminium-rich debris evidenced in Section 3.2.

Figs. 9a-c summarise the relationship between toluene alkylation activity, the porous properties of mesoporous zeolites derived from Z40-P (V_{micro}, S_{meso}, and V_{meso}), and treatment efficiency as a function of the NaOH concentration applied in their preparation. The negligible dependence of catalytic activity on the micropore volume is consistent with the access-limited

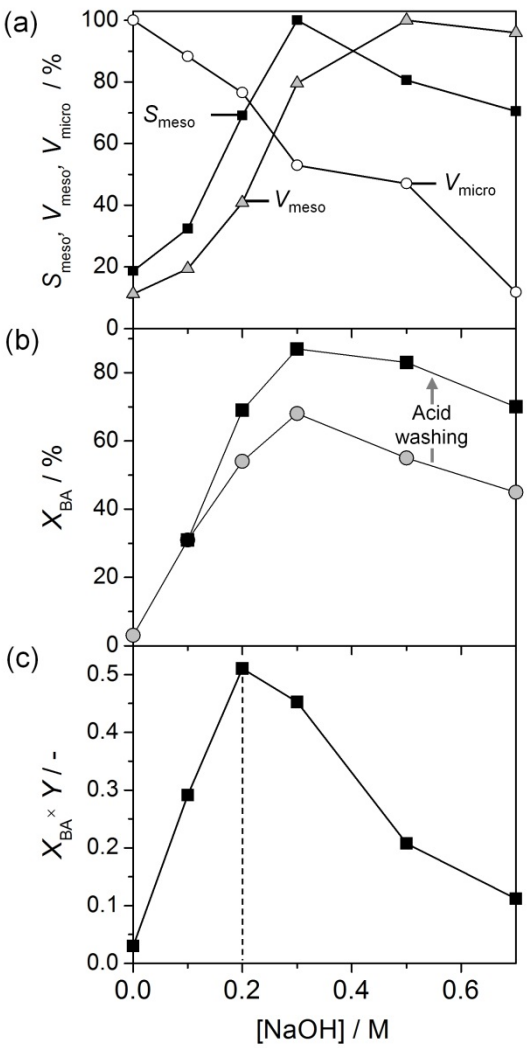

Fig. 9 Effect of the NaOH concentration on (a) the porous properties of the alkaline-treated Z40, (b) the conversion of benzyl alcohol during the alkylation with toluene over alkaline-treated (AT) zeolites before (grey circles) and after (solid squares) sequential acid washing (AW) after 10 min of reaction, and (c) the benzyl alcohol conversion factored by the overall treatment yield for the AT-AW zeolites. Values of the parent zeolite are represented at [NaOH] = 0 M. Reaction conditions as in caption of Fig. 5.

nature of the alkylation reaction. Accordingly, the strong interdependence between S_{meso} and X_{BA} is directly related to the larger surface area available for alkylation. The activity (X_{BA} at $t = 10$ min) mirrors the corresponding variation in the mesoporous surface area. Both reach a maximum for the sample treated at 0.3 M NaOH. In contrast, the trend in X_{BA} deviates from that of V_{meso}. This is most noticeable at increased values of mesopore volume, demonstrating that the generation of large mesopores is not advantageous in liquid-phase alkylation. Therefore, the mesopore surface seems a more suitable descriptor in the design of hierarchical zeolite catalysts than the mesopore volume. The positive impact of acid washing on the catalytic activity increased with the severity of the initial alkaline treatment (Fig. 9b). This further evidences the benefits of

This journal is © The Royal Society of Chemistry [year]

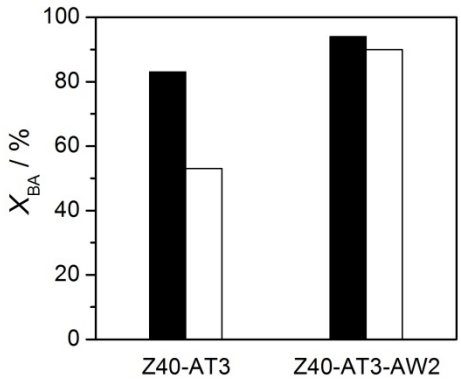

Fig. 10 Conversion of benzyl alcohol in the alkylation with toluene (solid bars) and cyclohexylbenzene (open bars) over hierarchical zeolites. Conditions: T = 433 K, P = 5 bar, t = 25 min, T/BA = 80, CHB/BA = 130, 0.6 wt.% zeolite.

removing the aluminium-rich debris which block potentially active Brønsted acid sites at the pore mouths. To account for the loss of raw material which occurs during preparation, the conversion of benzyl alcohol was factored by the treatment yield of hierarchical zeolites (Fig. 9c). Taking this into consideration, Z40-AT2-AW2, desilicated with 0.2 M NaOH, was identified as the optimal mesoporous zeolite catalyst derived from Z40-P in this study.

The catalytic properties of the hierarchical zeolites were also characterised in the alkylation of cyclohexylbenzene (Fig. 10). The larger substituted aromatic molecule was expected to provide even greater sensitivity to differences in the mesoporous surface structure than toluene. Remarkably, although the conversion of benzyl alcohol over Z40-AT3 was 30% lower than observed with toluene, the catalytic activity of Z40-AT3-AW2 (after 25 min) was nearly equivalent in both alkylations. This permitted further insight into the property-function relationships of the hierarchical zeolite catalysts. Acid sites present on the mesoporous surface of the modified zeolites have sufficient strength to catalyse both alkylation reactions. The higher conversions with toluene over the unwashed sample implied that residual aluminium species restrict access to active sites on the mesopore surface of alkaline-treated zeolites. The removal of such species by acid washing unblocks pore mouths and improves the active site accessibility, thereby reducing the molecular size-dependence of the catalytic activity. Comparatively, the relative enhancement of X_{BA} on mild acid treatment of Z40-AT3 was 9 and 45% for toluene and cyclohexylbenzene, respectively.

Consistent with previous work,[29] a clear trend is observed between alkylation activity and secondary mesoporosity (Fig. 11a). Interestingly, the linear dependence is distinct for zeolites obtained from Z15-P or Z40-P. This relates to the difference in framework aluminium content, which is 2.6 times higher in Z15-P. A three times larger mesoporous surface area is required to reach equivalent benzyl alcohol conversions for the Z40-derived hierarchical zeolites. This implies that mesoporosity introduction in aluminium-rich zeolites potentially offers greater catalytic improvements. The absence of any clear correlation with the bulk Si/Al ratio proves that moderately acidic species

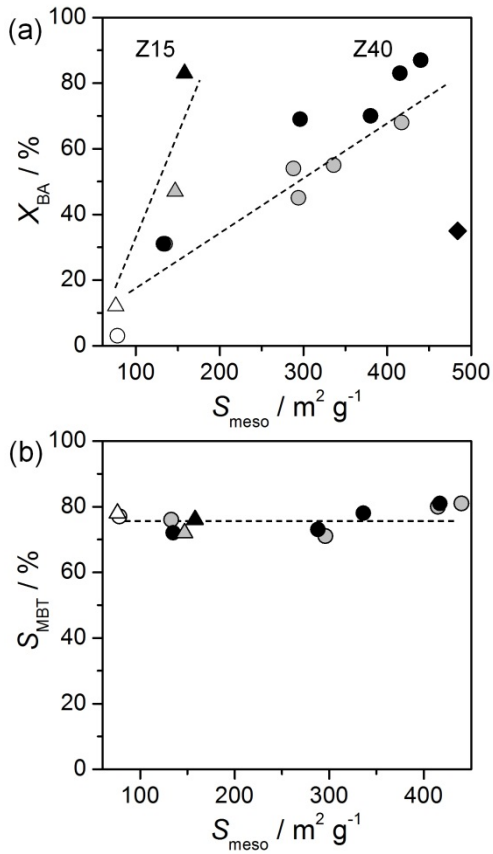

Fig. 11 (a) Conversion of benzyl alcohol and (b) selectivity to (methylbenzyl)benzene in the alkylation of toluene over zeolites derived from Z15-P (triangles) and Z40-P (circles) with respect to the mesoporous surface area (S_{meso}) after 10 min of reaction. Parent zeolites are indicated by open symbols, alkaline-treated by grey symbols, and acid-washed by black symbols. The black diamond symbol represents the drop in activity upon steaming of mesoporous Z40-AT3-AW2. Reaction conditions as in caption of Fig. 5.

residual from alkaline treatment are less active than framework aluminium in the context of alkylation. In addition, the amount of strong acid sites in the remaining zeolite framework is apparently unaffected by the treatments applied. The selectivity for (methylbenzyl)benzene was around 75%, independent of the bulk Si/Al ratio, the textural properties, or the presence of amorphous aluminium-rich debris (Fig. 11b). The main by-product of the reaction, dibenzyl ether (25%), results from the self-etherification of benzyl alcohol. Polyalkylated compounds were not observed, as expected from the use of an excess of toluene (T/BA = 80). The selectivity relationship between ortho, meta, and para isomers was estimated to be 4:1:5 for all zeolites. The similar selectivities verify that no shape selectivity effects, related to the participation of micropores, influence the product distribution. In agreement with our earlier observations, steaming significantly reduced the activity of the most active mesoporous zeolite (Z40-AT3-AW2 in Fig. 11a). However, the steamed sample retained a higher activity (X_{BA} = 35% after 10 min of reaction) than the best performing purely microporous zeolite.

The catalytic trends described in this work, have all been derived from liquid-phase alkylations of aromatic molecules. It

should be pointed out that these observations can differ for other reaction systems, with distinct acidity requirements, and extent of micropore utilisation, or under different process conditions. Furthermore, more detailed evaluation of the acidic properties is required to understand the variation in acid site speciation occurring upon post-synthetic modification. These aspects will be addressed in future work.

4. Conclusions

Both compositional and porosity variations induced by alkaline treatment contribute to the catalytic performance of desilicated ZSM-5 in the liquid-phase alkylation of toluene with benzyl alcohol. Textural development, which is best described in terms of mesoporous surface area, clearly dominates the overall catalytic performance of access-limited reactions. Larger pores, evidenced by high mesopore volumes and larger average pore diameters, were not beneficial in liquid-phase alkylation. In terms of compositional effects the efficiency of mesopore introduction in enhancing the catalytic activity is proportional to the framework density of aluminium in the parent zeolite. No relationship is found with the bulk Si/Al ratio. Aluminium-rich species residual from desilication block active sites at the external surface, impacting the activity improvement in the alkylation. The magnitude of this detrimental effect depends on the extent of dissolution and can be compensated by subsequent acid treatment. The catalytic knowledge gained in this study strengthens the ability to design hierarchical zeolites by desilication. This is achieved by defining the optimal starting zeolite and treatment conditions, and the requirement for acid washing.

Acknowledgements

ETH Zurich and the Swiss National Science Foundation (project number 200021-134572) are acknowledged for financial support.

Notes and references

Institute for Chemical and Bioengineering, Department of Chemistry and Applied Biosciences, ETH Zurich, Wolfgang-Pauli-Strasse 10, HCI E 125,CH-8093, Zurich, Switzerland. E-mail: jpr@chem.ethz.ch; Fax:+41 44 633 14 05

1. J. Kärger and D. Freunde, *Chem. Eng. Tech*., 2002, **25**, 769.
2. J. Pérez-Ramírez, C.H. Christensen, K. Egeblad, C.H. Christensen and J.C. Groen, *Chem. Soc. Rev.*, 2008, **37**, 2530.
3. R. Chal, C. Gérardin, M. Bulut and S. van Donk, *ChemCatChem*, 2011, **3**, 67.
4. W. Schmidt, *ChemCatChem*, 2009, **1**, 53.
5. M.S. Holm, E. Taarning, K. Egeblad and C.H. Christensen, *Catal. Today*, 2011, **168**, 3.
6. J. Čejka and S. Mintova, *Catal. Rev*., 2007, **49**, 457.
7. D. Verboekend and J. Pérez-Ramírez, *Catal. Sci. Technol.*, 2011, **1**, 879.
8. J. Pérez-Ramírez, S. Mitchell, D. Verboekend, M. Milina, N.-L. Michels, F. Krumeich, N. Marti and M. Erdmann, *ChemCatChem*, 2011, **3**, 1731.
9. D. Verboekend and J. Pérez-Ramírez, *Chem. Eur. J.*, 2011, **17**, 1137.
10. C. Fernandez, I. Stan, J.-P. Gilson, K. Thomas, A. Vicente, A. Bonilla and J. Pérez-Ramírez, *Chem. Eur. J.*, 2010, **16**, 6224.
11. D. Verboekend, S. Mitchell, M. Milina, J.C. Groen and J. Pérez-Ramírez, *J. Phys. Chem. C*, 2011, **115**, 14193.
12. D. Verboekend, A.M. Chabaneix, K. Thomas, J.-P. Gilson and J. Pérez-Ramírez, *CrystEngComm*., 2011, **13**, 3408.
13. P. Sazama, B. Wichterlova, J. Dedecek, Z. Tvaruzkova, Z. Musilova, L. Palumbo, S. Sklenak and O. Gonsiorova, *Microporous Mesoporous Mater*., 2011, **143**, 87.
14. D. Verboekend, L.A. Villaescusa, K. Thomas, I. Stan and J. Pérez-Ramírez, *Catal. Today*, 2010, **152**, 11.
15. S. Svelle, L. Sommer, K. Barbera, P.N.R. Vennestrøm, U. Olsbye, K.P. Lillerud, S. Bordiga, Y. Pan and P. Beato, *Catal. Today*, 2011, **168**, 38.
16. D. Verboekend, R. Caicedo-Realpe, A. Bonilla, M. Santiago and J. Pérez-Ramírez, *Chem. Mater.*, 2010, **22**, 4679.
17. J. Pérez-Ramírez, D. Verboekend, A. Bonilla and S. Abelló, *Adv. Funct. Mater.*, 2009, **19**, 3972.
18. Z. Musilová, N. Žilkova, S.-E. Park and J. Čejka, *Top Catal.*, 2010, **53**, 1457.
19. C.H. Christensen, K. Johannsen, E. Törnqvist, I. Schmidt, H. Topsøe and C.H. Christensen, *Catal. Today*, 2007, **128**, 117.
20. D.P. Serrano, R.A. García and D. Otero, *Appl. Catal. A*, 2009, **359**, 69.
21. D.R. Stull, *Ind. Eng. Chem.*, 1947, **39**, 517.
22. K.S. Pitzer and D.W. Scott, *J. Am. Chem. Soc.*, 1943, **65**, 803.
23. J. Klinowski, *Ann. Rev. Mater. Sci.*, 1988, **18**, 189.
24. A. Samoson, E. Lippmaa, G. Engelhardt, U. Lohse and H.-G. Jerschkewitz, *Chem. Phys. Lett.*, 1987, **134**, 589.
25. J.C. Groen, J.C. Jansen, J.A. Moulijn and J. Pérez-Ramírez, *J. Phys. Chem. B*, 2004, **108**, 13062.
26. M.S. Holm, S. Svelle, F. Joensen, P. Beato, C.H. Christensen, S. Bordiga and M. Bjørgen, *Appl. Catal.*, 2009, **356**, 23.
27. F. Thibault-Starzyk, I. Stan, S. Abelló, A. Bonilla, K. Thomas, C. Fernandez, J.-P. Gilson and J. Pérez-Ramírez, *J. Catal.*, 2009, **264**, 11.
28. R. Caicedo-Realpe and J. Pérez-Ramírez, *Microporous Mesoporous Mater.*, 2010, **128**, 91.
29. A.N.C. van Laak,. S.L. Sagala, J. Zečević, H. Friedrich, P.E. de Jongh and K.P. de Jong, *J. Catal.*, 2010, **276**, 170.

This journal is © The Royal Society of Chemistry [year]